Gold-Based Nanoparticles on Amino-Functionalized Mesoporous Silica Supports as Nanozymes for Glucose Oxidation

M. Carmen Ortega-Liebana [1,2,†], **Javier Bonet-Aleta** [1,2,3] , **Jose L. Hueso** [1,2,3,*] **and Jesus Santamaria** [1,2,3,*]

[1]   Institute of Nanoscience of Aragon (INA) and Department of Chemical and Environmental Engineering, C/Poeta Mariano Esquillor, s/n; Campus Rio Ebro, Edificio I+D, 50018 Zaragoza, Spain; mc.ortega@ed.ac.uk (M.C.O.-L.); jbaleta@unizar.es (J.B.-A.)
[2]   Networking Research Center on Bioengineering, Biomaterials and Nanomedicine (CIBER-BBN), 28029 Madrid, Spain
[3]   Instituto de Ciencia de Materiales de Aragon (ICMA); Consejo Superior de Investigaciones Cientificas (CSIC-University of Zaragoza), 50018 Zaragoza, Spain
*   Correspondence: jlhueso@unizar.es (J.L.H.); jesus.santamaria@unizar.es (J.S.)
†   Present address: Cancer Research UK Edinburgh Centre, University of Edinburgh, Crewe Road South, Edinburgh EH4 2XU, UK.

Abstract: The transformation of glucose represents a topic of great interest at different levels. In the first place, glucose is currently conceived as a green feedstock for the sustainable production of chemicals. Secondly, the depletion of glucose at the cellular level is currently envisioned as a promising strategy to treat and alter the erratic metabolism of tumoral cells. The use of natural enzymes offers multiple advantages in terms of specificity towards the glucose substrate but may lack sufficient robustness and recyclability beyond the optimal operating conditions of these natural systems. In the present work, we have evaluated the potential use of an inorganic based nanohybrid containing gold nanoparticles supported onto ordered mesoporous supports. We have performed different assays that corroborate the enzyme-mimicking response of these inorganic surrogates towards the selective conversion of glucose into gluconic acid and hydrogen peroxide. Moreover, we conclude that these enzyme-like mimicking surrogates can operate at different pH ranges and under mild reaction conditions, can be recycled multiple times and maintain excellent catalytic response in comparison with other gold-based catalysts.

Keywords: gold; nanozymes; enzyme-mimicking; glucose oxidation; mesoporous silica; surface functionalization

1. Introduction

Saccharides are abundant, renewable and sustainable chemical compounds that play a key role both at industrial level and in the metabolism of living beings [1,2]. Only in 2017, the United States produced about 27.5 M tons of starch, the most plentiful polysaccharide on Earth, which was further used for industrial and food applications. The hydrolysis of starch over supported metal catalysts produces glucose as main product. For this reason, from a green-feedstock point of view all selective chemical transformations of glucose are industrially attractive to produce high value-added products [1] and have been widely studied [1–4]. Glucose oxidation yielding gluconic acid possesses a huge industrial importance in the manufacturing of water-soluble cleansing products, food and beverages additives or pharmaceutics and cosmetics. Currently, this industrial production of

gluconic acid is achieved by fermentation using *Aspergillus niger* [3,5]. Enzyme-mediated processes face several drawbacks: (i) difficulties in recovery and recycling; (ii) high costs in product preparation and purification and (iii) the catalytic activity is often affected by minimal variations in the working environment [2,6].

Transformation of glucose is also extremely important in biomedicine and multiple cancer therapy studies are currently focused on glucose-starvation strategies to alter the local environment and metabolism of tumor cells [7,8]. For these reasons, there is an increasing interest in developing alternative enzyme-like catalysts based on inorganic materials that can overcome intrinsic limitations of natural enzymes [5–7,9–11]. Several nanomaterials [8,11] have been developed in the recent years aiming to emulate different kind of natural enzymes and so-called artificial enzymes or "nanozymes" [10–12]. Catalase-like materials are usually based on metals or metal oxides, such as Fe, Pt, Pd Ag or Au [4,6,11,13,14], which efficiently decompose H_2O_2 into H_2O and O_2. Cerium [6,9,10] and carbon-based nanomaterials such as fullerenes (C_{60}) [15,16] were remarkably efficient removing superoxide anion (O_2^-) yielding H_2O_2 and O_2, mimicking the activity of superoxide dismutase enzymes. Iron-based [11] and noble metal based (Au [17–19], Ag [20], Pt [21] or Pd [22]) nanomaterials have been widely reported as active catalysts to mimic peroxidase activity by oxidizing a substrate with H_2O_2. Finally, the enzyme-like oxidase mimicking activity represents another important field of current developments. Au [23], Pt [24] or Cu [25] nanomaterials can use O_2 to selectively oxidize a substrate, yielding H_2O_2 and the corresponding oxidation products. Nevertheless, the enzyme-like behavior for each material is affected by multiple and diverse factors, such as size, shape, pH, temperature or surface coating, among others [26].

The first catalysts tested in the catalytic oxidation of glucose using O_2 were Pd [26–28] and Pt [29–31] particles. Although some of them yielded >99% gluconic acid, these materials suffered from oxidation and critical deactivation caused by adsorption of reaction products. The introduction of Bi [32] partially avoided the previous problems, but their reusability was not evaluated. Among these inorganic enzyme surrogates, Au particles [4,23,33–44] have been the most studied material since early 2000s for the selective oxidation of glucose to gluconic acid. Gold is much more resistant to O_2 poisoning than previously cited elements [39] and reaction products have less affinity to adsorption process onto the Au surface [44] apart from being more active and selective [2,18,19]. However, the main drawback is the strong-dependence of catalytic activity on Au surface and particle size [44], being dramatically affected by sintering phenomena [37]. Typically, Au NPs-mediated catalytic oxidation of glucose (Scheme 1) is performed in neutral to basic medium (pH = 7–9). At this pH, the open and more reactive tautomer is promoted [28] and the protonation of carboxyl groups of the products is avoided, which may easily remain adsorbed onto Au surfaces [44]. While regular enzymatic pathways suggest the formation of an additional δ-gluconolactone intermediate [45], gold mimicking surrogates may follow other mechanisms involving a nucleophilic attack of Au–O⁻ sites that would ease the conversion into gluconic acid under milder experimental conditions [46].
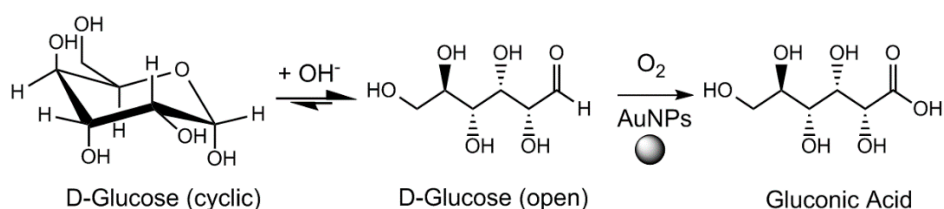
Scheme 1. pH dependent equilibrium and Au-mediated catalytic oxidation of glucose.

Analogously, temperature has also shown a positive impact on the rate and selectivity of the glucose oxidation reaction [44,47]. Although the use of a basic medium favors the glucose oxidation reaction and the stability of AuNPs [44], base-free conditions are still desired from the green chemistry, industrial and biomedicine point of view [47,48]. Therefore, it is necessary to improve the AuNPs

stability in absence of basic conditions with the selection of suitable stabilizing agents [48] or after immobilization in different functional supports [49].

Several supports have been used for Au NPs deposition and applied in the catalytic oxidation of glucose including carbon-based materials [38,50–53], Al_2O_3 [42,54], CeO_2 [38,39,52], ZrO_2 [55], TiO_2 [28,41], mesoporous SiO_2 [50] or polymers such as poly(methyl methacrylate), polystyrene or polyaniline [43], achieving in most of the cases >80% of glucose conversion and >90% selectivity for gluconic acid. The catalyst preparation method plays a key role in the catalytic activity [40]. The nature of Au-support interactions is also essential to ensure the stability of the catalytic system [36,56]. For instance, supports with high density of –OH groups on their surface promote the anchoring of Au NPs [27,57]. Likewise, $–NH_2$ surface functional groups can endorse stronger affinity with AuNPs by electrostatic attraction thereby resulting in a more efficient immobilization of both the active metallic nanoparticles and the glucose sustrate [58–60].

In this work, we describe the synthesis of an amino-functionalized mesoporous silica nanoplatform decorated with small gold nanoparticles immobilized by electrostatic attraction. This hybrid Au-silica nanohybrid has been evaluated as a potential enzyme surrogate with glucose-oxidase mimicking response. Multiple reaction conditions have been thoroughly explored to identify the best performing scenario and the main reaction products (i.e., gluconic acid and hydrogen peroxide) expected from the selective oxidation of glucose. Furthermore, this work addresses different colorimetric assays to identify these main reaction products and shows competitive catalytic results working under mild, environmentally friendly conditions that are favorable for environmental and biomedical targeted applications.

2. Results and Discussion

2.1. Synthesis and Characterization of Gold-Mesoporous Silica Heteronanostructures

Figure 1a summarizes the different synthesis stages required to fabricate the gold-based nanohybrids. The first step (denoted as (i) in Figure 1a) consisted on the preparation of the gold nanoparticles (Au-NPs). A phosphonium derived salt, tetrakis(hydroxymethyl) phosphonium chloride (THPC), was employed as reducing and stabilizing ligand of the Au NPs. The use of this ionic stabilizing agent has been previously reported by Duff et al. [61] and our group [49,62,63] as a successful alternative to poly-alcohols and other polymeric stabilizers with greater steric hindrance [62]. Cs-corrected Scanning Transmission Electron Microscopy (STEM) images demonstrated the formation of crystalline Au NPs with average diameters below 5 nm (Figure 1c). The second step (denoted as (ii) in Figure 1a) consisted on the synthesis of nanostructured silica hosts containing ordered mesoporous channels as demonstrated by TEM inspection (Figure 1d,e). These silica spheres were functionalized with an amino-grafting agent (see the Materials and Methods section for further details) containing $–NH_2$ terminal groups (~8% wt. according to thermogravimetric analysis and considered optimal to keep a good colloidal and thermal stability [59,64]) and Si-O bonds able to attach on the surface of the silica spheres [49,65,66].

The final step (see (iii) in Figure 1a) involved the gold seeding of the amino-functionalized silica hosts favored by the electrostatic attraction of positively charged $–NH_3^+$ terminal groups and negatively charged Au NPs [49,59,65,66]. The negative charge of these type of Au NPs has been previously reported [67,68] and tentatively attributed to the coexistence of $Au–O^-$ surface bonds and chloride stabilizing ions [67–69]. TEM and STEM images (Figure 1f,g) confirmed the successful attachment of the Au NPs. Pore size restrictions limited the loading of the bigger Au NPs within the mesochannels. ICP analysis confirmed 1% Au wt. loadings. Following this strategy, Au NPs are endowed with higher catalytic sites availability while preventing them from partially coarsening events typically observed in freestanding Au NPs of this nature [63]. Furthermore, providing a solid and stable silica support can facilitate the recovery of the catalytic Au NPs for their potential reusability and/or regeneration [59].
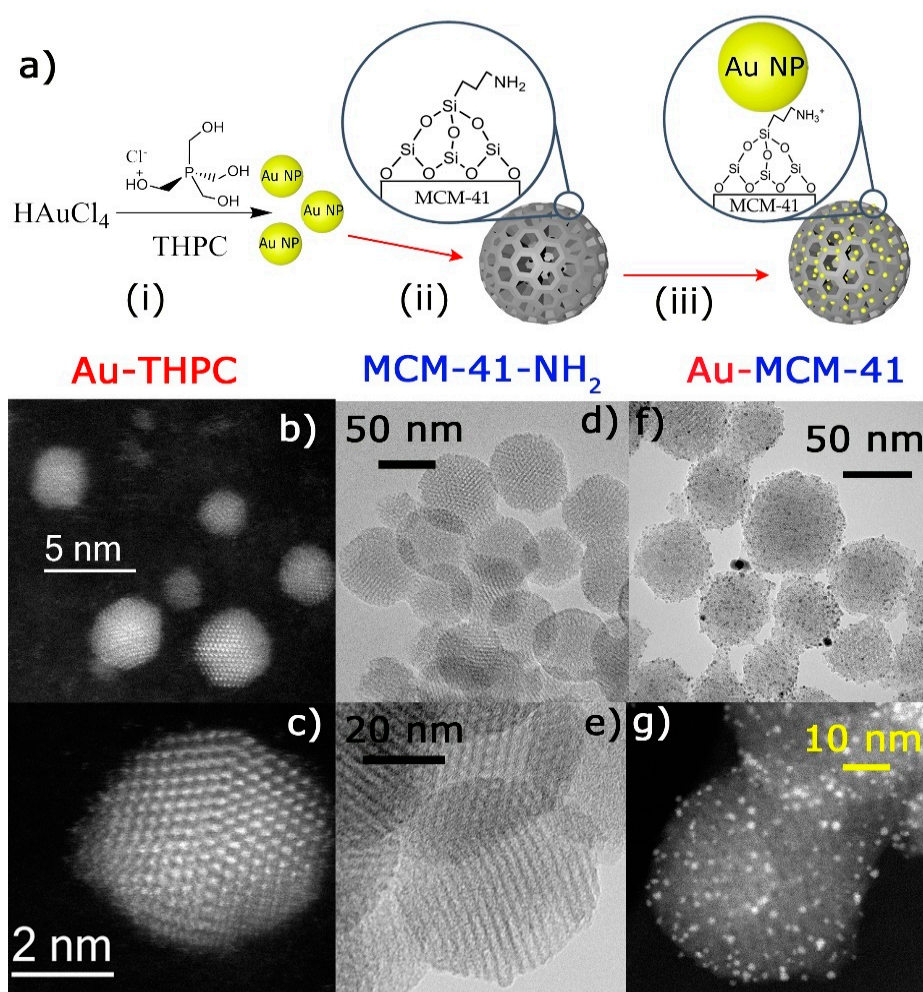
Figure 1. Synthesis and characterization of the Au-mesoporous silica hybrids: (**a**) Schematic description of the different synthesis stages including (i) the synthesis of the Au NPs with the aid of THPC [59,62]; (ii) the synthesis of the MCM-41 ordered mesoporous spheres and the amino-grafting step with APTES [49,65,66]; (iii) the gold seeding attachment by electrostatic attraction; (**b**–**c**) HAADF-STEM images of the individual Au NPs; (**d**–**e**) TEM images at different magnifications of the mesoporous silica supports showing the ordered organization of the mesochannels; (**f**–**g**) TEM and STEM images displaying the correct gold seeding process via electrostatic attraction and the formation of the Au-silica hybrid nanoparticles.

2.2. Evaluation of Au-MCM-41 Nanohybrids as Enzyme-Mimicking Surrogates Towards Glucose Oxidation

2.2.1. Colorimetric Assays to Determine the Oxidation of Glucose into Gluconic Acid

Au-MCM-41 hybrids were evaluated as inorganic structured materials mimicking the action of the natural enzyme glucose oxidase (GOx). Our enzyme-like surrogates were tested towards the aerobic oxidation of glucose under mild reaction conditions.

In order to evaluate the successful conversion of glucose into gluconic acid (hereafter GA) and hydrogen peroxide (H_2O_2) (the expected reaction products), a combination of different colorimetric assays were carried out while exploring the influence of different experimental variables. First of all, formation of GA was indirectly validated by UV-Vis spectroscopy. GA can selectively react with hydroxylamine and a trivalent iron salt form a red-colored hydroxamate complex with a broad absorption centered at 505 nm (see Figure 2a,c) [12,70].
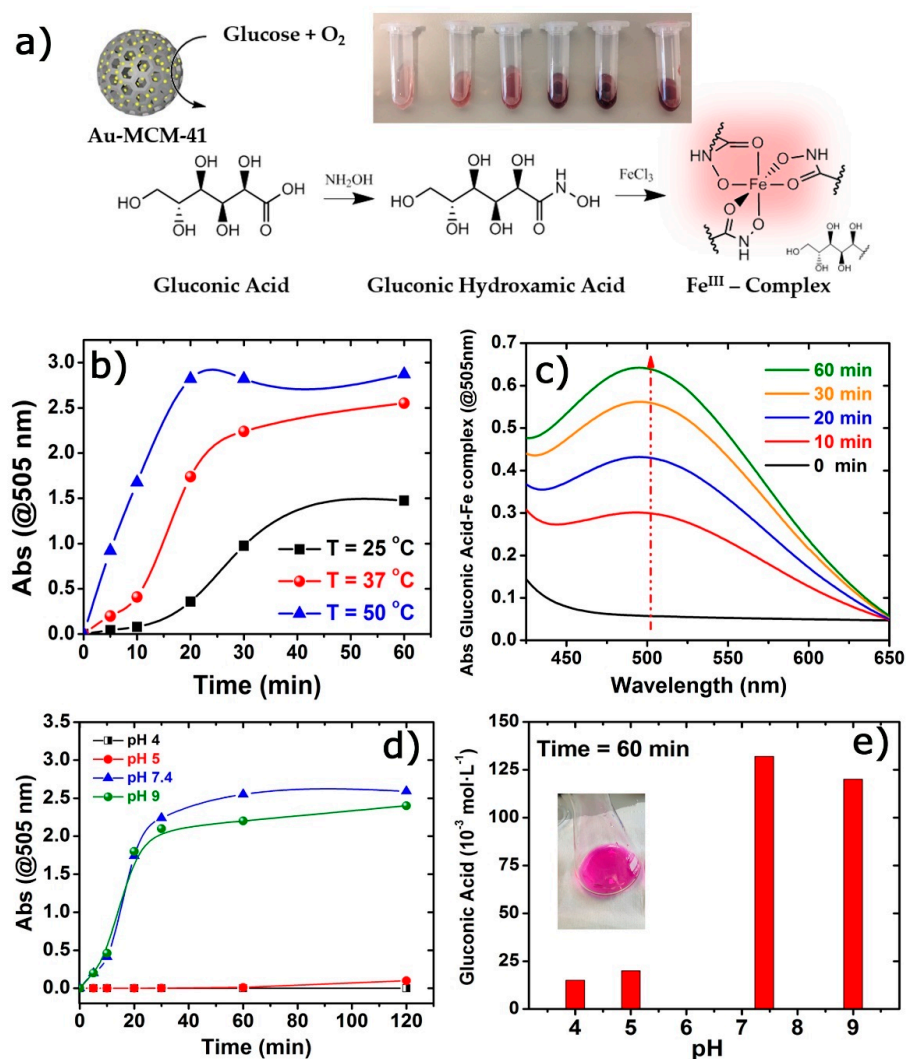
Figure 2. Determination of the presence of gluconic acid as one of the expected products retrieved from the oxidation of glucose in the presence of the enzyme-like gold-silica nanocatalyst: (**a**) Schematic display of the reaction of gluconic acid with hydroxylamine and trivalent Fe salt to form a red colored Fe-hydroxamate complex with a maximum absorbance centered at 505 nm (inset: digital image showing the evolution of the red-colored vials upon increasing reaction times related to increasing formation of gluconic acid); (**b**) Comparison of the maximum absorbance detected at different time intervals with different reaction temperatures and neutral pH = 7.4; (**c**) Representative UV-Vis spectra of the Fe-complex exhibiting an increase in the maximum absorbance centered at 505 nm after different reaction time intervals; (**d**) Comparison of the maximum absorbance detected at different time intervals and different pH conditions (temperatures fixed at 37 °C); (**e**) Concentrations of gluconic acid determined after colorimetric titration with NaOH and phenolphthalein as indicator (inset: digital image of the final color obtained after completing the neutralization of the gluconic acid with NaOH using phenolphthalein as colorimetric indicator). Experimental conditions: [catalyst] = 0.025 mg/mL; [glucose] = 150 mM; reaction media buffered with 0.2 M sodium acetate/acetic acid. Titration experiments were carried out using titration controls with known concentrations of commercial gluconic acid at pH adjusted to 4.

The progressive formation of the Fe-complex was monitored at different reaction times under neutral pH conditions. Figure 2b shows the positive influence of increasing the reaction temperature from 25 to 50 °C to increase the selective oxidation of glucose into GA that readily reacts to form the colored complex (see inset in Figure 2a,b). Likewise, the influence of the pH was further evaluated at a fixed reaction temperature of 37 °C. Figure 2d shows the evolution of the absorption band of the

hydroxamate complex at different pH values and confirms poorer performance of the Au-MCM-41 catalyst under basic conditions. It is also worth noting that no additional evolution was observed after 60 min of reaction. The formation and quantification of GA as reaction product was additionally determined by a colorimetric titration with sodium hydroxide and phenolphthalein [50,71]. According to the amounts of GA generated (see Figure 2e), the glucose conversion levels reached up to 85% at neutral pH conditions and T = 37 °C after 45 min of reaction. Titration methods confirmed the lower response under more acidic conditions as previously shown by UV-Vis spectroscopy (Figure 2d).

2.2.2. Colorimetric Assays to Identify the Formation of Hydrogen Peroxide

The other main reaction product expected from an enzyme-like glucose oxidase activity is typically hydrogen peroxide (Figure 3a). In order to assess its presence, two different colorimetric assays were performed [12]. The H_2O_2 generated during the oxidation of glucose was initially reduced with the aid of a horseradish peroxidase (HRP) enzyme (Figure 3a). In the first colorimetric assay, this reduction step induced the simultaneous oxidation of 3,3,5,5-tetramethylbenzidine (hereafter TMB) into its blueish colored derivative with a maximum absorption at 652 nm (Figure 3a,c). The systematic evaluation of the glucose oxidation under different pH conditions rendered a similar trend as observed for the detection of gluconic acid (*vide infra* Figure 3d). Neutral and basic media ensured the best time-dependent catalytic response of the Au-MCM-41 nanohybrids and the highest absorption values for the TMB(ox) dye (Figure 3b,c).
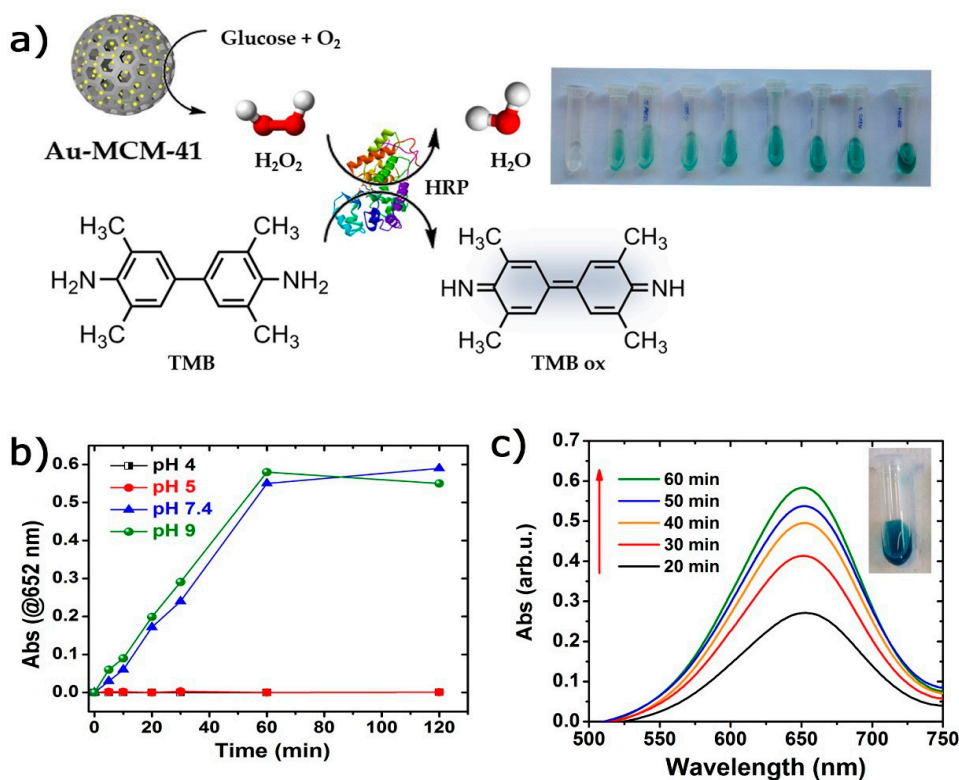

Figure 3. Colorimetric determination of the presence of hydrogen peroxide as reaction product retrieved from the glucose oxidation reaction (TMB assay): (**a**) Schematic display of the formation of hydrogen peroxide and its subsequent redox reaction mediated by a horseradish enzyme that readily reacts with TMB to render the blue colored oxidized derivative with maximum absorption spectrum centered at 652 nm; (inset: digital image showing the evolution of the blue-colored vials upon increasing reaction times related to increasing formation of H_2O_2); (**b**) Time-dependent evolution of the maximum absorption

of TMB(ox) at different pH conditions and keeping reaction temperatures of 37 °C; (**c**) Representative UV-Vis spectra of the TMBox dye after increasing reaction times (inset: digital image of the final solution after 60 min reaction); Experimental conditions: [catalyst] = 0.025 mg/mL; [glucose] = 150 mM; reaction media buffered with 0.2 M sodium acetate/acetic acid.

An analogous colorimetric assay mediated by the HRP enzyme to promote the simultaneous oxidation of a 2,2-azino-bis (3-ethylbenzothiozoline)-6-sulfonic acid salt (ABTS) into its blue colored oxidized derivative was also carried out (see scheme in Figure 4a). A similar behavior regarding the pH influence over time could be observed (Figure 4b). No catalytic activity could be detected at lower pH values of 4 or 5. Furthermore, no additional evolution of the maximum absorption spectrum at 415 nm (Figure 4c) was detected beyond the first 60 min of reaction under neutral or basic conditions (Figure 4b).
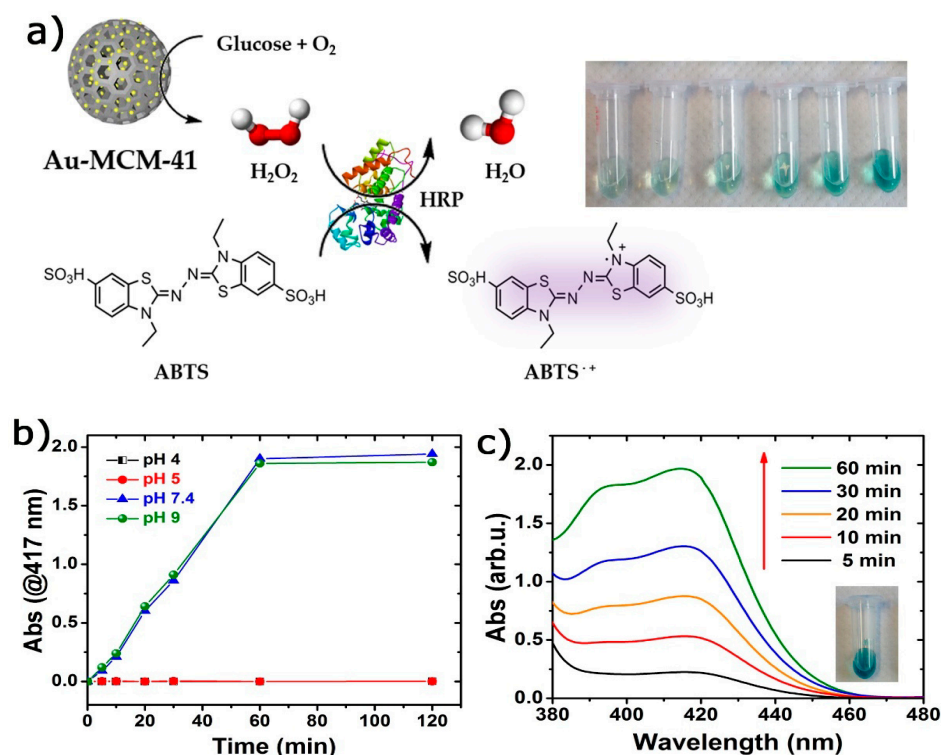

Figure 4. Colorimetric determination of the presence of hydrogen peroxide as reaction product retrieved from the glucose oxidation reaction (using the ABTS mediated assay): (**a**) Schematic display of the formation of hydrogen peroxide and its subsequent redox reaction mediated by a horseradish enzyme that readily reacts with ABTS to render the blue colored oxidized derivative with maximum absorption spectrum centered at 415 nm; (inset: digital image showing the evolution of the blue-colored vials upon increasing reaction times related to increasing formation of H_2O_2); (**b**) Time-dependent evolution of the maximum absorption of ABTS(ox) at different pH conditions and keeping reaction temperatures of 37 °C; (**c**) Representative UV-Vis spectra of the ABTS(ox) molecule at increasing reaction time intervals; Experimental conditions: [catalyst] = 0.025 mg/mL; [glucose] = 150 mM; reaction media buffered with 0.2 M sodium acetate/acetic acid.

2.2.3. Steady-State Kinetics and Recyclability Evaluation

To quantify the glucose-oxidase enzyme mimicking activity of the Au-MCM-41 nanocatalyst, a kinetic study of the glucose conversion into gluconic acid was carried out. The kinetic parameters were determined after performing a series of experiments with increasing concentrations of glucose (Figure 5a) and adjusting the gluconic acid generated after 30 min of reaction by quantitative colorimetric assays that included pH titration [50,71] and UV-Vis spectroscopy [70,72] (see Experimental section for

further details). The data were fitted to a non-linear regression of the Michaelis-Menten equation and the apparent kinetic parameters were obtained using the Lineweaver-Burk double reciprocal plot as previously suggested by Gao et al. [73] (see inset in Figure 5a).
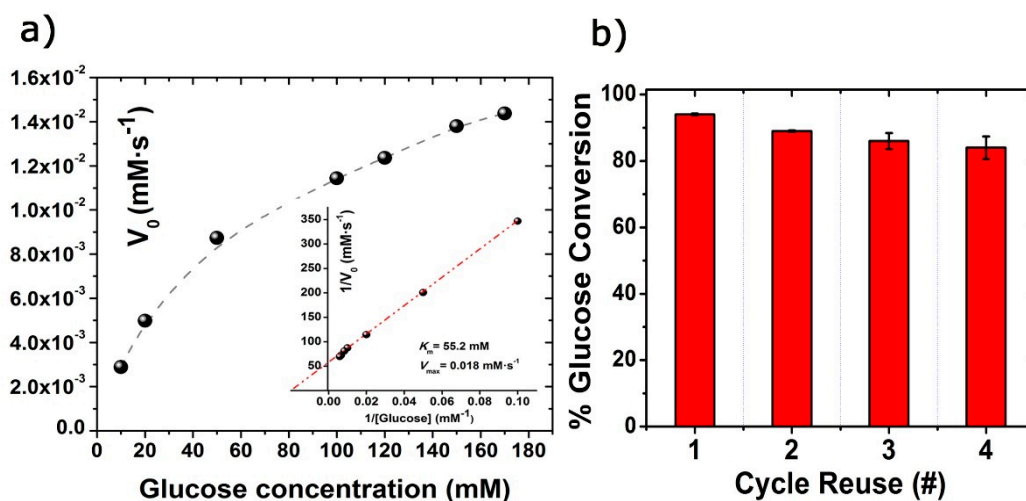

Figure 5. (**a**) Steady-state kinetic assay and evaluation of the conversion rates of glucose in the presence of the enzyme-like gold-silica nanocatalyst using different substrate concentrations (fixed concentrations of glucose: 10, 20, 50, 100, 120, 150, 180 mM). The formation of Fe-hydroxamate complex after 30 min was evaluated for each concentration to plot the apparent reaction rate (V_o) and $1/V_o$; (inset: double-reciprocal plots of the glucose-oxidase mimicking activity of the nanocatalyst assuming a Lineweaver-Burk plot). Experimental details: [glucose] = 10–180 mM; [catalyst] = 0.025 mg/mL; pH = 7.4 in 0.2 M acetate/acetic buffer; temperature: 37 °C. (**b**) Reusability of the enzyme-like gold-silica nanocatalyst after 4 consecutive cycles. Experimental details: [glucose] = 150 mM; [catalyst] = 0.025 mg/mL; pH = 7.4 in 0.2 M acetate/acetic buffer; temperature: 37 °C; the nanocatalyst was recovered by centrifugation.

An apparent Michaelis-Menten constant (defined as K_m) of ~55 mM and a maximum velocity (V_{max}) of 18×10^{-6} M/s were determined (inset graph in Figure 5a). This apparent K_m constant is higher than other values reported for freestanding gold nanozymes (K_m ~7 mM) [71], polymer-coated gold mimics (K_m ~0.4 mM) [19], gold-supported mimicking systems (K_m ~27 mM) [50] or the glucose oxidase (GOx) natural enzyme (K_m ~5 mM) [71]. According to this value, our Au-MCM-41 nanozymes show a slightly weaker affinity towards the glucose substrate [19,50,71]. Nevertheless, the corresponding catalytic activity (K_{cat}) defined by the coefficient V_{max}/[concentration of catalyst] improves the values reported for natural GOx (K_{cat} ~14.2 s^{-1} vs. K_{cat} ~9.7 s^{-1}, respectively) and it is close to freestanding Au NPs (K_{cat} ~18.5 s^{-1}) reported by Luo et al. [71]. From the catalytic standpoint, the enzyme-like Au-MCM-41 nanohybrids exhibit a very positive response probably due to the good accessibility and homogeneous distribution of the gold active sites in the mesoporous support. The glucose conversion levels achieved (85–92% in less than 1 h of reaction) working under mild reaction conditions (in the absence of co-solvents or basic conditions and without high temperature or working pressure) are extremely competitive with current gold-based systems available in the literature and briefly summarized in Table 1 (*vide infra*).

It is also plausible that a controlled O_2 feeding would have led to an even better performance. Still, it is a very positive outcome if a potential application to modify the microenvironment of tumoral cells (with low O_2 concentration levels) is envisioned. As suggested by Cattaneo et al. [46] it is quite plausible that the reaction of glucose is strongly favored by the nucleophilic attack of glucose on Au–O$^-$ sites. This reaction would be favored at higher pH and temperatures but those requirements would be still less demanding than those reported in the regular enzymatic pathway, where the hydrolysis of the δ-glucono-lactone is the rate-limiting step for gluconic acid generation [45]. Even though the

final product is the same, the Au-based nanozyme may follow a different mechanism. Additional insights with the aid of Nuclear Magnetic Resonance (NMR) techniques and theoretical simulation studies can be noteworthy for the corroboration of these differences in reaction mechanisms between natural enzyme and artificial enzyme systems [45,46,53,74–76]. Furthermore, the silica mesoporous support provides not only a great active surface area for the accommodation of glucose but also a more favorable platform to facilitate the recovery and reutilization of the nanozyme than in freestanding systems. Figure 5b illustrates the capability of these Au-silica hybrids to be reutilized in multiple consecutive reaction cycles with a minimal reduction of the glucose conversion levels, most likely attributable to an incomplete retrieval of all the catalyst from cycle to cycle.

Table 1. Selection of Au-based catalysts reported for glucose oxidation.

Catalyst	Glucose/Au (mol/mol)	[Glucose]$_0$	O$_2$ (mL/min)	T (°C)	pH	%Conversion (react. time)	Ref.
1.0% Au/C	100	0.20 M	20	40	BF [b]	80.0 (18 h)	[38]
1.0% Au/C	1000	0.22 M	20	50	9.5	100 (50 min)	[23,55]
0.5% Au/C	40,000	3.00 M	100	50	9.5	95.0 (55 min)	[55,77]
1.0% Au/NPC	32,000	0.30 M	120	50	9.0	>99.0	[40]
2.0% Au/C	100	0.20 M	0.1 MPa	40	BF	78.0 (18 h)	[38]
0.9% Au/CMK	1050 [a]	0.10 M	0.3 MPa	110	BF	92.0 (2 h)	[53]
1.0% Au/Al$_2$O$_3$	32,000	0.30 M	120	50	9.0	100 (15 min) [a]	[35]
1.6% Au/Al$_2$O$_3$	100	0.20 M	20	120	BF	78.0 (18 min)	[39]
0.3% Au/Al$_2$O$_3$	-	0.10 M	500	40	9.0	100	[33]
2.0% Au-Mt/CeAl	100	0.20 M	0.1 MPa	120	BF	>75 (16 h)	[78]
1.0% Au/ZrO$_2$	32,000	0.30 M	120	50	9.0	100 (12 min) [a]	[35]
Au/TiNT	100	0.25 M	SP 5 bar	80	9.5	73.0 (6 h)	[27]
AuPd/TiNT	100	0.25 M	SP 5 bar	80	9.5	74.4 (6 h)	[27]
0.5%Au/TiO$_2$	1000	0.10 M	1 MPa	110	BF	92.0 (2 h)	[42]
3.9% Au/CeO$_2$	100	0.20 M	20	120	BF	70.0 (18 h)	[39]
0.9%Au/meso SiO$_2$	1080 [a]	0.10 M	0.3 MPa	110	BF	67.0 (2 h)	[53]
1.0%Au/MCM-41	118,200	0.15 M	-	37	7.4	85.0 (45 min)	This work

[a] Calculated from the reference; [b] Base-free.

3. Materials and Methods

3.1. Chemicals

Chemicals were used as received without further purification. Gold(III) chloride hydrate (HAuCl$_4$·3H$_2$O, 50% Au basis), Tetrakis(hydroxymethyl) phosphonium chloride solution (THPC, 80 wt%, Aldrich, Germany), Sodium hydroxide (NaOH), Hexadecyltrimethylammonium bromide (CTABr, 96%), Tetraethyl orthosilicate (TEOS, ≥99.0%, GC), (3-aminopropyl)triethoxysilane (APTES, 99%), Triethanolamine (TEA, ≥ 99.0%, GC), D-(+)-glucose (ACS reagent), Peroxidase from horseradish (type VI-A), 2,2-azino-bis (3-ethylbenzothiozoline)-6-sulfonic acid diammonium salt (ABTS-(NH$_4$)$_2$), 98% HPLC), 3,3,5,5-tetramethylbenzidine (TMB, 99%), Iron (III) chloride hexahydrate (97%), hydroxylamine solution (50 wt% H$_2$O, 99.999%) were purchased from Sigma-Aldrich, Germany). Sodium hydroxide solutions were kept in well-washed polyethylene containers, and chloroauric acid solutions were excluded from the light. The solutions were prepared using ultrapure water which was purified by a Millipore Milli-Q system (Merck, Madrid, Spain).

3.2. Synthesis of Gold Nanoparticles Using THPC as Reducing and Stabilizing Agent (Au-NPs)

Ultrasmall Au-NPs were prepared as described previously elsewhere with slight modifications [62,63]. Successive charging of a 50 mL glass vial, while stirring, with 14 mL of distilled water and then, in order, portions of aqueous solutions of sodium hydroxide (1 M, 165 μL), the reducing agent THPC (65 mM, 333 μL), and the freshly dissolved chloroauric acid salt (3 mg, 1 mL) results in the formation of orange-brown hydrosols of gold. Two minutes was allowed between the addition of THPC and that

of chloroauric acid. The reaction mixture was stirred for 1 day at room temperature, protecting the mixture from light to prevent the photothermal decomposition of precursors [79]. Finally, the resulting colloid Au-NPs were stored in a refrigerator at 4 °C until further use.

3.3. Synthesis of Amino-Functionalized Mesoporous Silica Supports (MCM-41 Type Material)

Silica materials with hexagonally arranged uniform mesopores were synthesized using the previously reported approach [59,80,81] for base catalysed sol gel condensation of TEOS in the presence of structure directing agent. MCM-41-like mesoporous nanoparticles were synthesized by the following procedure: CTAB (1.00 g, 2.7 mmol) was first dissolved in deionized water (1 L). NaOHaq. (2.00 M, 5 mL) was added to the CTAB solution, and the temperature was adjusted to 80 °C. TEOS (7 mL, 0.05 mmol) was then added drop-wise to the surfactant solution. The mixture was left to stir for 3 h to give a white precipitate. The solid product was centrifuged and washed with deionized water until a neutral pH. Finally, the solid was dried. To prepare the final porous material, the as-synthesized solid were dissolved in acidic EtOH (100 mL, and few drops of HCl 37%) for 12 h to remove the template phase. The precipitate was recovered by centrifugation at 20,000 g and thoroughly washed with distilled H_2O/EtOH (1:1, 2x) and EtOH (2x). Then the product was dried overnight under reduced pressure. Subsequently, primary amine groups were grafted on the surface of the mesochannels by condensation of 3-aminopropyltriethoxysilane (APTES), to favor electrostatic interactions between the MCM-41 nanoparticles and the Au-NPs [49,59,65,82]. Briefly, 0.50 g of MCM-41 material was dispersed in 10 mL of toluene, 100 μL of TEA and 200 μL of APTES. The reaction was refluxed for 24 h, and the product was centrifuged and washed twice prior to total drying under vacuum for further use.

3.4. Synthesis of the Au-MCM-41 Nanohybrids

To prepare the gold-silica nanohybrid, 0.10 g of amino modified MCM-41 nanoparticles was dispersed in 10 mL of the Au-NCs stored suspension. The suspension was adjusted to pH 5 and stirred at 20 °C for 12 h in the dark. Subsequently, the product was collected by centrifugation, washed several times with water, and re-dispersed in water until further use. The synthesis of materials has been performed by the Platform of Production of Biomaterials and Nanoparticles of the NANOBIOSIS ICTS, more specifically by the Nanoparticle Synthesis Unit of the CIBER in BioEngineering, Biomaterials & Nanomedicine (CIBER-BBN).

3.5. Determination of Activity and Steady-State Kinetics of the Au-MCM-41 Nanohybrids

The glucose oxidation reactions were carried out with temperature control in a thermoplate, equipped with a mechanical stirrer operating at 750 rpm, using a total volume of 100 mL and different glucose concentrations from 10 up to 180 mM. The concentration of the Au-MCM-41 nanocatalyst was 0.025 mg/mL. Concentration of dissolved O_2 was typically in the range of 6–8 mg/L (determined with an Orion Optical Dissolved O_2 sensor, Thermo Scientific). The pH of the reaction mixture was held constant at 7.4. The kinetics of the catalytic reaction could be well adjusted to a typical Michaelis–Menten curve [70,72]. The Michaelis–Menten constant was calculated using the Lineweaver–Burk plot: $1/V_0 = (K_m/V_{max}) \cdot (1/[S]) + (1/V_{max})$, where V_0 is the initial velocity, V_{max} is the maximal reaction velocity, and [S] is the concentration of the substrate. The rate of the catalytic reaction was defined as the amount of generated product, gluconic acid, in a fixed time interval of 30 min. The concentration of gluconic acid was determined via titration with NaOH (0.1 M) using phenolphthalein at pH 8.2 as colorimetric pH indicator. Likewise, this reaction product, (i.e., gluconic acid), was also verified by reaction with hydroxylamine and a trivalent Fe^{III} salt, leading to a red complex hydroxamate-Fe^{3+} (with a maximum absorbance at 505 nm) [70]. Namely, 125 μL of solution 1 (5 mmol/L EDTA and 0.15 mmol/L triethylamine in water) and 12.5 μL of solution 2 (3 mol/L NH_2OH in water) were added to 200 μL of the supernatant centrifuged reaction solution, and the mixture was allowed to react for 25 min. Finally, 62.5 μL of solution 3 (1 mol/L HCl, 0.1 mol/L $FeCl_3$, and 0.25 mol/L CCl_3COOH in water) was added to the reaction medium, and reaction was incubated for another 5 min before spectral

acquisition. Absorbance values from the Fe-complex at different reaction times and total gluconic acid concentrations were correlated using the Lambert-Beer law and a molar absorption coefficient of 61.2 [50,70–72]. In order to prevent the influence of the nanoparticles, the suspensions were previously centrifuged at 6000 rpm in 2 mL Eppendorfs.

Hydrogen peroxide (H_2O_2) was indirectly tested with the aid of a horseradish peroxidase (HRP) enzyme that selectively favored the reduction of the H_2O_2 present in solution and the simultaneous oxidation of ABTS or TMB with specific absorbances at 415 and 652 nm, respectively [12,70,72]. In a standard procedure, 300 μL of the filtered catalytic reaction solution was added to 50 μL of 8 mM ABTS and 50 μL of 0.4 μg/mL HRP. The oxidation produced a green color with a major absorbance peak at 415 nm (final concentrations after dilutions for UV-Vis measurements were 1 mM ABTS and 0.05 μg/mL HRP). Also, 350 μL of the filtered catalytic reaction solution was added to 8 μL of 40 mM TMB and 50 μL of 0.4 μg/mL HRP (final concentrations after dilutions for UV-Vis measurements were 0.8 mM TMB and 0.05 μg/mL HRP). The oxidation produced a blue color with a maximum absorbance centered at 652 nm. Acetate/Acetic acid buffer solutions (0.2 M, 0.2 mL) were prepared combining 5.4 g sodium acetate trihydrate +1.2 mL glacial acetic acid in 198.8 mL water. Recycling experiments carried out after one hour reaction runs included 2 centrifuge cycles and redispersion in water prior to the addition of fresh glucose solutions. This process was repeated prior to each reuse.

3.6. Catalyst Characterization

The textural properties of the MCM-41 materials were determined from nitrogen adsorption isotherms measured by an ASAP 2020 instrument (Micromeritics, Norcross, GA, USA). The samples were out-gassed at 26.7 Pa and 623 K for 6 h before the measurement. The amount of amine groups grafted onto silica surface was determined by thermogravimetric analysis (SDTA-851 equipment, Mettler Toledo, Barcelona, Spain). Samples of ca. 3 mg were heated at 5 °C/min up to 800 °C) under synthetic air flow. The morphologies, size distribution and crystalline structure of these materials were determined by Transmission Electron Microscopy (TEM) in a T20 (Tecnai, Thermo Fisher, Hillboro, OR, USA) and Titan Cube (FEI, Thermo Fisher, Hillboro, OR, USA) system operated at 200–300 kV, respectively, and coupled with a CCD camera (Gatan, CA, USA). The samples for TEM analysis were prepared by suspension of the corresponding sample in water, dropping the suspension onto a 200-mesh carbon-coated copper grid (Electron Microscopy Sciences, Hatfield, PA, USA) and letting it dry under ambient air with the aid of anti-capillary tweezers. The UV-vis absorption spectra of the products of reaction were systematically recorded using a V-67 UV/Visible spectrophotometer (JASCO, Madrid, Spain) using a quartz cell of 1 cm light path.

4. Conclusions

Au NPs supported onto mesoporous silica supports via electrostatic attraction represents a feasible and straightforward strategy to fabricate glucose-oxidase enzyme-like inorganic platforms able to deliver a successful performance under mild reaction conditions (neutral pH and temperature).

Conflicts of Interest: The authors declare no conflict of interest.

References

1. Gallezot, P. Conversion of biomass to selected chemical products. *Chem. Soc. Rev.* **2012**, *41*, 1538–1558. [CrossRef] [PubMed]
2. Kobayashi, H.; Fukuoka, A. Synthesis and utilisation of sugar compounds derived from lignocellulosic biomass. *Green Chem.* **2013**, *15*, 1740–1763. [CrossRef]
3. Xue, Z.; Ma, M.-G.; Li, Z.; Mu, T. Advances in the conversion of glucose and cellulose to 5-hydroxymethylfurfural over heterogeneous catalysts. *RSC Adv.* **2016**, *6*, 98874–98892. [CrossRef]
4. Kusema, B.T.; Murzin, D.Y. Catalytic oxidation of rare sugars over gold catalysts. *Catal. Sci. Technol.* **2013**, *3*, 297–307. [CrossRef]
5. Pal, P.; Kumar, R.; Banerjee, S. Manufacture of gluconic acid: A review towards process intensification for green production. *Chem. Eng. Process. Process. Intensif.* **2016**, *104*, 160–171. [CrossRef]
6. Wu, J.J.X.; Wang, X.Y.; Wang, Q.; Lou, Z.P.; Li, S.R.; Zhu, Y.Y.; Qin, L.; Wei, H. Nanomaterials with enzyme-like characteristics (nanozymes): Next-generation artificial enzymes (II). *Chem. Soc. Rev.* **2019**, *48*, 1004–1076. [CrossRef]
7. Yu, S.; Chen, Z.; Zeng, X.; Chen, X.; Gu, Z. Advances in nanomedicine for cancer starvation therapy. *Theranostics* **2019**, *9*, 8026–8047. [CrossRef]
8. Huo, M.; Wang, L.; Chen, Y.; Shi, J. Tumor-selective catalytic nanomedicine by nanocatalyst delivery. *Nat. Commun.* **2017**, *8*, 357. [CrossRef]
9. Baldim, V.; Bedioui, F.; Mignet, N.; Margaill, I.; Berret, J.F. The enzyme-like catalytic activity of cerium oxide nanoparticles and its dependency on Ce^{3+} surface area concentration. *Nanoscale* **2018**, *10*, 6971–6980. [CrossRef]
10. Lin, Y.H.; Ren, J.S.; Qu, X.G. Catalytically Active Nanomaterials: A Promising Candidate for Artificial Enzymes. *Acc. Chem. Res.* **2014**, *47*, 1097–1105. [CrossRef]
11. Gao, L.Z.; Zhuang, J.; Nie, L.; Zhang, J.B.; Zhang, Y.; Gu, N.; Wang, T.H.; Feng, J.; Yang, D.L.; Perrett, S.; et al. Intrinsic peroxidase-like activity of ferromagnetic nanoparticles. *Nat. Nanotechnol.* **2007**, *2*, 577–583. [CrossRef]
12. Jiang, D.W.; Ni, D.L.; Rosenkrans, Z.T.; Huang, P.; Yan, X.Y.; Cai, W.B. Nanozyme: New horizons for responsive biomedical applications. *Chem. Soc. Rev.* **2019**, *48*, 3683–3704. [CrossRef]
13. Li, L.; Yang, Z.; Fan, W.; He, L.; Cui, C.; Zou, J.; Tang, W.; Jacobson, O.; Wang, Z.; Niu, G.; et al. In Situ Polymerized Hollow Mesoporous Organosilica Biocatalysis Nanoreactor for Enhancing ROS-Mediated Anticancer Therapy. *Adv. Funct. Mater.* **2019**. [CrossRef]
14. Fan, L.; Tian, Y.; Lou, D.; Wu, H.; Cui, Y.; Gu, N.; Zhang, Y. Catalytic gold–platinum alloy nanoparticles and a novel glucose oxidase mimic with enhanced activity and selectivity constructed by molecular imprinting. *Anal. Methods* **2019**, *11*, 4586–4592.
15. Li, J.; Liu, W.; Wu, X.; Gao, X. Mechanism of pH-switchable peroxidase and catalase-like activities of gold, silver, platinum and palladium. *Biomaterials* **2015**, *48*, 37–44. [CrossRef]
16. Ali, S.S.; Hardt, J.I.; Quick, K.L.; Kim-Han, J.S.; Erlanger, B.F.; Huang, T.-T.; Epstein, C.J.; Dugan, L.L. A biologically effective fullerene (C60) derivative with superoxide dismutase mimetic properties. *Free Radic. Biol. Med.* **2004**, *37*, 1191–1202. [CrossRef]
17. Wu, Y.-S.; Huang, F.-F.; Lin, Y.-W. Fluorescent Detection of Lead in Environmental Water and Urine Samples Using Enzyme Mimics of Catechin-Synthesized Au Nanoparticles. *ACS Appl. Mater. Interfaces* **2013**, *5*, 1503–1509. [CrossRef]
18. Shen, X.M.; Liu, W.Q.; Gao, X.J.; Lu, Z.H.; Wu, X.C.; Gao, X.F. Mechanisms of Oxidase and Superoxide Dismutation-like Activities of Gold, Silver, Platinum, and Palladium, and Their Alloys: A General Way to the Activation of Molecular Oxygen. *J. Am. Chem. Soc.* **2015**, *137*, 15882–15891. [CrossRef]
19. Fan, L.; Lou, D.D.; Wu, H.A.; Zhang, X.Z.; Zhu, Y.F.; Gu, N.; Zhang, Y. A Novel AuNP-Based Glucose Oxidase Mimic with Enhanced Activity and Selectivity Constructed by Molecular Imprinting and O-2-Containing Nanoemulsion Embedding. *Adv. Mater. Interfaces* **2018**, *5*, 1801070. [CrossRef]
20. Chen, L.; Sha, L.; Qiu, Y.; Wang, G.; Jiang, H.; Zhang, X. An amplified electrochemical aptasensor based on hybridization chain reactions and catalysis of silver nanoclusters. *Nanoscale* **2015**, *7*, 3300–3308. [CrossRef]

21. Wu, G.-W.; He, S.-B.; Peng, H.-P.; Deng, H.-H.; Liu, A.-L.; Lin, X.-H.; Xia, X.-H.; Chen, W. Citrate-Capped Platinum Nanoparticle as a Smart Probe for Ultrasensitive Mercury Sensing. *Anal. Chem.* **2014**, *86*, 10955–10960. [CrossRef]

22. Lan, J.; Xu, W.; Wan, Q.; Zhang, X.; Lin, J.; Chen, J.; Chen, J. Colorimetric determination of sarcosine in urine samples of prostatic carcinoma by mimic enzyme palladium nanoparticles. *Anal. Chim. Acta* **2014**, *825*, 63–68. [CrossRef]

23. Biella, S.; Prati, L.; Rossi, M. Selective Oxidation of D-Glucose on Gold Catalyst. *J. Catal.* **2002**, *206*, 242–247. [CrossRef]

24. Li, L.; Zhang, L.; Carmona, U.; Knez, M. Semi-artificial and bioactive ferroxidase with nanoparticles as the active sites. *Chem. Commun.* **2014**, *50*, 8021–8023. [CrossRef]

25. Periasamy, A.P.; Roy, P.; Wu, W.-P.; Huang, Y.-H.; Chang, H.-T. Glucose Oxidase and Horseradish Peroxidase Like Activities of Cuprous Oxide/Polypyrrole Composites. *Electrochim. Acta* **2016**, *215*, 253–260. [CrossRef]

26. Zhang, H.; Lu, L.; Kawashima, K.; Okumura, M.; Haruta, M.; Toshima, N. Synthesis and Catalytic Activity of Crown Jewel-Structured (IrPd)/Au Trimetallic Nanoclusters. *Adv. Mater.* **2015**, *27*, 1383–1388. [CrossRef]

27. Khawaji, M.; Zhang, Y.; Loh, M.; Graça, I.; Ware, E.; Chadwick, D. Composition dependent selectivity of bimetallic Au-Pd NPs immobilised on titanate nanotubes in catalytic oxidation of glucose. *Appl. Catal. B Environ.* **2019**, *256*, 117799. [CrossRef]

28. Zhang, X.; Shi, H.; Chi, Q.; Liu, X.; Chen, L. Cellulose-supported Pd nanoparticles: Effective for the selective oxidation of glucose into gluconic acid. *Polym. Bull.* **2019**, *77*, 1003–1014. [CrossRef]

29. Comotti, M.; Pina, C.D.; Rossi, M. Mono- and bimetallic catalysts for glucose oxidation. *J. Mol. Catal. A Chem.* **2006**, *251*, 89–92. [CrossRef]

30. Jin, X.; Zhao, M.; Shen, J.; Yan, W.; He, L.; Thapa, P.S.; Ren, S.; Subramaniam, B.; Chaudhari, R.V. Exceptional performance of bimetallic Pt$_1$Cu$_3$/TiO$_2$ nanocatalysts for oxidation of gluconic acid and glucose with O$_2$ to glucaric acid. *J. Catal.* **2015**, *330*, 323–329. [CrossRef]

31. Zhang, H.; Toshima, N. Preparation of novel Au/Pt/Ag trimetallic nanoparticles and their high catalytic activity for aerobic glucose oxidation. *Appl. Catal. A Gen.* **2011**, *400*, 9–13. [CrossRef]

32. Bönnemann, H.; Brijoux, W.; Tilling, A.S.; Siepen, K. Application of heterogeneous colloid catalysts for the preparation of fine chemicals. *Top. Catal.* **1997**, *4*, 217–227. [CrossRef]

33. Baatz, C.; Decker, N.; Pruse, U. New innovative gold catalysts prepared by an improved incipient wetness method. *J. Catal.* **2008**, *258*, 165–169. [CrossRef]

34. Greer, A. Christopher Foote's discovery of the role of singlet oxygen O-1(2) ((1)Delta(g)) in photosensitized oxidation reactions. *Acc. Chem. Res.* **2006**, *39*, 797–804. [CrossRef]

35. Ishida, T.; Kinoshita, N.; Okatsu, H.; Akita, T.; Takei, T.; Haruta, M. Influence of the support and the size of gold clusters on catalytic activity for glucose oxidation. *Angew. Chem. Int. Ed. Engl.* **2008**, *47*, 9265–9268. [CrossRef]

36. Benkó, T.; Beck, A.; Geszti, O.; Katona, R.; Tungler, A.; Frey, K.; Guczi, L.; Schay, Z. Selective oxidation of glucose versus CO oxidation over supported gold catalysts. *Appl. Catal. A Gen.* **2010**, *388*, 31–36. [CrossRef]

37. Cao, Y.; Liu, X.; Iqbal, S.; Miedziak, P.J.; Edwards, J.K.; Armstrong, R.D.; Morgan, D.J.; Wang, J.; Hutchings, G.J. Base-free oxidation of glucose to gluconic acid using supported gold catalysts. *Catal. Sci. Technol.* **2016**, *6*, 107–117. [CrossRef]

38. Megías-Sayago, C.; Bobadilla, L.F.; Ivanova, S.; Penkova, A.; Centeno, M.A.; Odriozola, J.A. Gold catalyst recycling study in base-free glucose oxidation reaction. *Catal. Today* **2018**, *301*, 72–77. [CrossRef]

39. Megías-Sayago, C.; Ivanova, S.; López-Cartes, C.; Centeno, M.A.; Odriozola, J.A. Gold catalysts screening in base-free aerobic oxidation of glucose to gluconic acid. *Catal. Today* **2017**, *279*, 148–154. [CrossRef]

40. Okatsu, H.; Kinoshita, N.; Akita, T.; Ishida, T.; Haruta, M. Deposition of gold nanoparticles on carbons for aerobic glucose oxidation. *Appl. Catal. A Gen.* **2009**, *369*, 8–14. [CrossRef]

41. Baatz, C.; Pruse, U. Preparation of gold catalysts for glucose oxidation by incipient wetness. *J. Catal.* **2007**, *249*, 34–40. [CrossRef]

42. Guo, S.; Fang, Q.; Li, Z.; Zhang, J.; Zhang, J.; Li, G. Efficient base-free direct oxidation of glucose to gluconic acid over TiO2-supported gold clusters. *Nanoscale* **2019**, *11*, 1326–1334. [CrossRef]

43. Ishida, T.; Kuroda, K.; Kinoshita, N.; Minagawa, W.; Haruta, M. Direct deposition of gold nanoparticles onto polymer beads and glucose oxidation with H2O2. *J. Colloid Interface Sci.* **2008**, *323*, 105–111. [CrossRef]

44. Jv, Y.; Li, B.; Cao, R. Positively-charged gold nanoparticles as peroxidase mimic and their application in hydrogen peroxide and glucose detection. *Chem. Commun.* **2010**, *46*, 8017–8019. [CrossRef]

45. Pocker, Y.; Green, E. Hydrolysis of d-glucono-delta-lactone. I. General acid-base catalysis, solvent deuterium-isotope effects, and transition-state characterization. *J. Am. Chem. Soc.* **1973**, *95*, 113–119. [CrossRef]

46. Cattaneo, S.; Stucchi, M.; Villa, A.; Prati, L. Gold Catalysts for the Selective Oxidation of Biomass-Derived Products. *ChemCatChem* **2018**, *11*, 309–323. [CrossRef]

47. Prüße, U.; Herrmann, M.; Baatz, C.; Decker, N. Gold-catalyzed selective glucose oxidation at high glucose concentrations and oxygen partial pressures. *Appl. Catal. A Gen.* **2011**, *406*, 89–93. [CrossRef]

48. Prüße, U.; Heidinger, S.; Baatz, C. Catalytic conversion of renewables: Kinetic and mechanistic aspects of the gold-catalyzed liquid-phase glucose oxidation. *vTI Agric. For. Res.* **2011**, *16*, 261–272.

49. Zieba, M.; Hueso, J.L.; Arruebo, M.; Martinez, G.; Santamaria, J. Gold-coated halloysite nanotubes as tunable plasmonic platforms. *New J. Chem.* **2014**, *38*, 2037–2042. [CrossRef]

50. Lin, Y.; Li, Z.; Chen, Z.; Ren, J.; Qu, X. Mesoporous silica-encapsulated gold nanoparticles as artificial enzymes for self-activated cascade catalysis. *Biomaterials* **2013**, *34*, 2600–2610. [CrossRef]

51. Beltrame, P.; Comotti, M.; Della Pina, C.; Rossi, M. Aerobic oxidation of glucose II. Catalysis by colloidal gold. *Appl. Catal. A-Gen.* **2006**, *297*, 1–7. [CrossRef]

52. Wang, Y.; Van de Vyver, S.; Sharma, K.K.; Román-Leshkov, Y. Insights into the stability of gold nanoparticles supported on metal oxides for the base-free oxidation of glucose to gluconic acid. *Green Chem.* **2014**, *16*, 719–726. [CrossRef]

53. Qi, P.; Chen, S.; Chen, J.; Zheng, J.; Zheng, X.; Yuan, Y. Catalysis and Reactivation of Ordered Mesoporous Carbon-Supported Gold Nanoparticles for the Base-Free Oxidation of Glucose to Gluconic Acid. *ACS Catal.* **2015**, *5*, 2659–2670. [CrossRef]

54. Comotti, M.; Della Pina, C.; Matarrese, R.; Rossi, M. The catalytic activity of "naked" gold particles. *Angew. Chem. Int. Ed. Engl.* **2004**, *43*, 5812–5815. [CrossRef]

55. Della Pina, C.; Falletta, E.; Prati, L.; Rossi, M. Selective oxidation using gold. *Chem. Soc. Rev.* **2008**, *37*, 2077–2095. [CrossRef] [PubMed]

56. Comotti, M.; Pina, C.D.; Matarrese, R.; Rossi, M.; Siani, A. Oxidation of alcohols and sugars using Au/C catalysts. *Appl. Catal. A Gen.* **2005**, *291*, 204–209. [CrossRef]

57. Khawaji, M.; Chadwick, D. Au-Pd Bimetallic Nanoparticles Immobilised on Titanate Nanotubes: A Highly Active Catalyst for Selective Oxidation. *ChemCatChem* **2017**, *9*, 4353–4363. [CrossRef]

58. Datta, K.K.R.; Reddy, B.V.S.; Ariga, K.; Vinu, A. Gold Nanoparticles Embedded in a Mesoporous Carbon Nitride Stabilizer for Highly Efficient Three-Component Coupling Reaction. *Angew. Chem. Int. Ed.* **2010**, *49*, 5961–5965. [CrossRef]

59. Miguel-Sancho, N.; Martinez, G.; Sebastian, V.; Malumbres, A.; Florea, I.; Arenal, R.; Ortega-Liebana, M.C.; Hueso, J.L.; Santamaria, J. Pumping Metallic Nanoparticles with Spatial Precision within Magnetic Mesoporous Platforms: 3D Characterization and Catalytic Application. *ACS Appl. Mater. Interfaces* **2017**, *9*, 41529–41536. [CrossRef]

60. Ortega-Liebana, M.C.; Hueso, J.L.; Ferdousi, S.; Arenal, R.; Irusta, S.; Yeung, K.L.; Santamaria, J. Extraordinary sensitizing effect of co-doped carbon nanodots derived from mate herb: Application to enhanced photocatalytic degradation of chlorinated wastewater compounds under visible light. *Appl. Catal. B Environ.* **2017**, *218*, 68–79. [CrossRef]

61. Duff, D.G.; Baiker, A.; Edwards, P.P. A new hydrosol of gold clusters. *J. Chem. Soc. Chem. Commun.* **1993**, 96–98. [CrossRef]

62. Hueso, J.L.; Sebastian, V.; Mayoral, A.; Uson, L.; Arruebo, M.; Santamaria, J. Beyond gold: Rediscovering tetrakis-(hydroxymethyl)-phosphonium chloride (THPC) as an effective agent for the synthesis of ultra-small noble metal nanoparticles and Pt-containing nanoalloys. *RSC Adv.* **2013**, *3*, 10427–10433. [CrossRef]

63. Uson, L.; Sebastian, V.; Mayoral, A.; Hueso, J.L.; Eguizabal, A.; Arruebo, M.; Santamaria, J. Spontaneous formation of Au-Pt alloyed nanoparticles using pure nano-counterparts as starters: A ligand and size dependent process. *Nanoscale* **2015**, *7*, 10152–10161. [CrossRef] [PubMed]

64. Talavera-Pech, W.A.; Esparza-Ruiz, A.; Quintana-Owen, P.; Vilchis-Nestor, A.R.; Carrera-Figueiras, C.; Avila-Ortega, A. Effects of different amounts of APTES on physicochemical and structural properties of amino-functionalized MCM-41-MSNs. *J. Sol Gel Sci. Technol.* **2016**, *80*, 697–708. [CrossRef]

65. Gomez, L.; Hueso, J.L.; Ortega-Liebana, M.C.; Santamaria, J.; Cronin, S.B. Evaluation of gold-decorated halloysite nanotubes as plasmonic photocatalysts. *Catal. Commun.* **2014**, *56*, 115–118. [CrossRef]

66. Uson, L.; Hueso, J.L.; Sebastian, V.; Arenal, R.; Florea, I.; Irusta, S.; Arruebo, M.; Santamaria, J. In-Situ preparation of ultra-small Pt nanoparticles within rod-shaped mesoporous silica particles: 3-D tomography and catalytic oxidation of n-hexane. *Catal. Commun.* **2017**, *100*, 93–97. [CrossRef]

67. Vogel, W.; Duff, D.G.; Baiker, A. X-ray structure of a new hydrosol of gold clusters. *Langmuir* **1995**, *11*, 401–404. [CrossRef]

68. Westcott, S.L.; Oldenburg, S.J.; Lee, T.R.; Halas, N.J. Formation and adsorption of clusters of gold nanoparticles onto functionalized silica nanoparticle surfaces. *Langmuir* **1998**, *14*, 5396–5401. [CrossRef]

69. Pfeiffer, C.; Rehbock, C.; Huhn, D.; Carrillo-Carrion, C.; de Aberasturi, D.J.; Merk, V.; Barcikowski, S.; Parak, W.J. Interaction of colloidal nanoparticles with their local environment: The (ionic) nanoenvironment around nanoparticles is different from bulk and determines the physico-chemical properties of the nanoparticles. *J. R. Soc. Interface* **2014**, *11*, 20130931. [CrossRef]

70. Ortega-Liebana, M.C.; Hueso, J.L.; Arenal, R.; Santamaria, J. Titania-coated gold nanorods with expanded photocatalytic response. Enzyme-like glucose oxidation under near-infrared illumination. *Nanoscale* **2017**, *9*, 1787–1792. [CrossRef]

71. Luo, W.J.; Zhu, C.F.; Su, S.; Li, D.; He, Y.; Huang, Q.; Fan, C.H. Self-Catalyzed, Self-Limiting Growth of Glucose Oxidase-Mimicking Gold Nanoparticles. *ACS Nano* **2010**, *4*, 7451–7458. [CrossRef] [PubMed]

72. Ortega-Liebana, M.C.; Hueso, J.L.; Fernandez-Pacheco, R.; Irusta, S.; Santamaria, J. Luminescent mesoporous nanorods as photocatalytic enzyme-like peroxidase surrogates. *Chem. Sci.* **2018**, *9*, 7766–7778. [CrossRef] [PubMed]

73. Liu, S.H.; Lu, F.; Xing, R.M.; Zhu, J.J. Structural Effects of Fe_3O_4 Nanocrystals on Peroxidase-Like Activity. *Chem.-Eur. J.* **2011**, *17*, 620–625. [CrossRef]

74. Cheng, P.; Wang, H.; Shi, X. The effect of phenylalanine ligands on the chiral-selective oxidation of glucose on Au(111). *Nanoscale* **2020**, *12*, 3050–3057. [CrossRef] [PubMed]

75. Ishchuk, O.P.; Sterner, O.; Strevens, H.; Ellervik, U.; Manner, S. The use of polyhydroxylated carboxylic acids and lactones to diminish biofilm formation of the pathogenic yeast Candida albicans. *RSC Adv.* **2019**, *9*, 10983–10989. [CrossRef]

76. Zhang, Y.A.; Jin, Y.L.; Cui, H.X.; Yan, X.Y.; Fan, K.L. Nanozyme-based catalytic theranostics. *RSC Adv.* **2020**, *10*, 10–20. [CrossRef]

77. Comotti, M.; Dellapina, C.; Falletta, E.; Rossi, M. Is the biochemical route always advantageous? The case of glucose oxidation. *J. Catal.* **2006**, *244*, 122–125. [CrossRef]

78. Chenouf, M.; Megías-Sayago, C.; Ammari, F.; Ivanova, S.; Centeno, M.; Odriozola, J. Immobilization of Stabilized Gold Nanoparticles on Various Ceria-Based Oxides: Influence of the Protecting Agent on the Glucose Oxidation Reaction. *Catalysts* **2019**, *9*, 125. [CrossRef]

79. Heutz, N.A.; Dolcet, P.; Birkner, A.; Casarin, M.; Merz, K.; Gialanella, S.; Gross, S. Inorganic chemistry in a nanoreactor: Au/TiO_2 nanocomposites by photolysis of a single-source precursor in miniemulsion. *Nanoscale* **2013**, *5*, 10534–10541. [CrossRef]

80. Balas, F.; Manzano, M.; Colilla, M.; Vallet-Regi, M. L-Trp adsorption into silica mesoporous materials to promote bone formation. *Acta Biomater.* **2008**, *4*, 514–522. [CrossRef]

81. Manzano, M.; Aina, V.; Arean, C.O.; Balas, F.; Cauda, V.; Colilla, M.; Delgado, M.R.; Vallet-Regi, M. Studies on MCM-41 mesoporous silica for drug delivery: Effect of particle morphology and amine functionalization. *Chem. Eng. J.* **2008**, *137*, 30–37. [CrossRef]

82. Eguizabal, A.; Uson, L.; Sebastian, V.; Hueso, J.L.; Pina, M.P. Efficient and facile tuning of Vulcan XC72 with ultra-small Pt nanoparticles for electrocatalytic applications. *RSC Adv.* **2015**, *5*, 90691–90697. [CrossRef]